Preparation and characterization of quinary nitrate salt based composite phase change material with low melting point for low and medium temperature thermal energy storage

Chuan Li [a], Guoyun Leng [a], Li Han [a], Qi Li [a,*], Haitao Lu [a], Rongyu Xu [a], Zhang Bai [b,*], Yanping Du [c], Yuting Wu [a]

[a] MOE Key Laboratory of Enhanced Heat Transfer and Energy Conservation, Beijing Key Laboratory of Heat Transfer and Energy Conversion, Beijing University of Technology, Beijing 100124, China

[b] College of New Energy, China University of Petroleum (East China), Qingdao 266580, China

[c] School of Engineering, Lancaster University, Lancaster LA1 4YW, UK

*Corresponding author: liqi@bjut.edu.cn; baizhang@upc.edu.cn

Abstract

This work concerns the development of a shape-stable molten salt based composite phase change material (PCM) for low and medium temperature thermal energy storage. The composite was is fabricated by using the cold compression and hot sintering method with the employment of a eutectic quinary nitrate salt of $NaNO_3$-$NaNO_2$-KNO_3-KNO_2-$LiNO_3$ as PCM, halloysite nanotube (HNT) as skeleton supporting material and natural graphite as thermal conductivity enhancement additive. A sequence of characterizations was is performed to investigate the composite microstructure, chemical and physical compatibility, thermal stability, phase change behaviour, and thermal conductivity as well as cycling performance. The results indicate that an excellent chemical compatibility has been achieved among the ingredients of quinary salt, HNT and graphite within the composite. A mass concentration of 50 wt.% HNT endows the composite with the optimal formulation in which 10 wt.% graphite can be successfully accommodated and a thermal conductivity around 1.31 W/m·K can be acquired. Moreover, in such a formulation, the composite presents a considerably low melting temperature of 72.4 °C and a high thermal decomposition temperature of 530 °C, which achieves the composite a relatively high energy storage density nearly 500 kJ/kg at a temperature range of 25-510 °C. The results presented in this work demonstrate that the quinary salt-HNT-graphite composite with fairly low phase transition temperature and a splendid combination of thermal properties and cycling performance could be a promising candidate to replace the conventional organic based PCMs utilized in low temperature thermal energy storage fields.

Keywords: Quinary nitrate salt; Composite phase change material; Shape stability; Thermal energy storage; Low melting temperature;

1. Introduction

It has been universally agreed that the development of energy storage technology could be able to eliminate the imbalance of energy supply and demand, and to achieve stable power output [1-3]. Thermal energy storage (TES) as one of highly efficient energy storage technologies refers to a transition process that store the surplus energy through the forms of either heat, cold or their

combinations, and has presented tremendous application potential in the consumption of renewable energy and utilization of industrial waste heat [4, 5]. Of the three modes of TES, the latent heat storage using phase change material (PCM) has drawn huge attentions in last decades owning to its advantages of quasi-isothermal melting-solidifying process and large heat storage capacity, and has been utilized in many fields such as cold chain logistics transport, building energy efficient heating and mobile energy recovery and storage as well as peak shaving of energy networks, to name but a few [6, 7].

Molten salts as one of promising candidates have been broadly used in medium and high TES fields due to their merits of opportune melting temperature, high energy storage capacity, and favourable thermal stability as well as low cost [8-10]. However, the wide-scale use of molten salt has been restricted to a certain extent because of the two main issues of poor thermal conductivity and chemical instability. A large number of investigations have indicated that the fabrication of a so-called shape stability phase change composite provides solutions towards these two challenges. Such a form-stable composite usually contains a molten salt for heat storage, a skeleton supporting material (SSM) for maintaining structure stability and a thermal conductivity additive (TCA) for performance enhancement, and have presented to be able to achieve outstanding thermal and mechanical properties [5, 7-9]. Zhang et al. [11, 12] prepared a phase change composite using a solar salt as PCM and an open-cell SiC ceramic as SSM, and it was found that the composite thermal conductivity can be significantly improved by the conduction-friendly porous skeleton. Due to the greater influence of thermal conduction induced by SiC ceramic than the natural convection, the heat transfer rate within the composite can be boosted by nearly 42%. Wang et al. [13] investigated a ternary chloride salt composite by using a porous Si_3N_4 as SSM, and they found over 88% salt can be accommodated in the composite. Because of the highly thermal conductivity of ceramic substance, the composite thermal conductivity can enhance by six times greater than the pure ternary salt. Meanwhile, excellent chemical stability had also achieved in the composite and stable thermophysical properties were measured even though the composite went through 300 thermal cycles. Miliozzi et al. [14] fabricated a concrete/diatomite/solar salt composite with the aim to utilize the combined sensible and latent heat for thermal energy storage, and their results indicated that the addition of 2% solar salt into the cement mortar could achieve positive impacts on the composite thermal and mechanical properties. Using steel slag as SSM, Liu et al. [15] synthesized a nitrate salt composite. It was revealed that more than 50 wt.% salt could be able to accommodate inside the composite, and in such a composition, the composite achieved a thermal conductivity of 0.68 W/m·K. Lu et al. [16] evaluated a ternary nitrate salt composite by employing expanded graphite as SSM and they affirmed that a splendid chemical stability has been achieved between the nitrate salt and SSM. Although the use of expanded graphite enhanced the thermal conductivity of the composite, the thermal decomposition temperature was reduced. With the use of carbide slag as SSM, Xiong et al. [17, 18] developed a Na_2CO_3 based composite and it was indicated that the carbonate salt can be successfully encapsulated by the carbide slag to form shape-stable composite. A mass fraction of 52.5 wt.% endowed the composite with the optimal behaviour in which a mechanical strength over 22 MPa and a thermal conductivity over 0.6 W/m·K can be obtained.

From the above literature reviews, it can be asserted that the research focuses on the employment of cold compression-hot sintering method for fabrication of salt composite have been mainly on the development of shape stability materials for medium-high temperature applications, and very little

investigation has been reported on the synthesis of molten salt composite for low temperature thermal energy storage. Jiang et al. [19] proposed a quaternary nitrate salt composite and demonstrated that the composite was suitable for low temperature application owning to their low melting point around 103 °C. Our previous work [20] studied a nitrate salt based composite by using MgO as SSM, and it was declared that a fairly low melting point around 90 °C and high decomposition temperature over 620 °C had been achieved in the composite. These investigations indicate that the use of either ternary or quaternary salt as PCM for composite fabrication can bring down the material melting temperature, thereby making them to be satisfied in applications of low temperature thermal energy storage. However, this is inadequate since there will be existence of large temperature fluctuation scenarios such as industrial and construction waste heat recovery where the main temperature is concentrated on 70-80 °C while the maximum temperature could be higher than 300-400 °C. This part of the residual heat could not be recycled by using of the traditional organic-polymer composites due to the its inherent issue of low decomposition temperature (typically <250 °C). This brings out the major motivation of this investigation, in which a quinary nitrate salt composite was developed and investigated. It is demonstrated that the salt composite achieves an extremely low melting point around 72 °C and a high thermal decomposition temperature over 500 °C that could be used in low and medium thermal energy storage fields. To fabricate such salt composite, a halloysite nanotube (HNT) was employed as SSM. The HNT has been broadly utilized for preparation of low-temperature organic composites but very little has been done in accommodating molten salt. Herein we reported that such ceramic nanotube could be able to employed as skeleton substance for the fabrication of quinary salt composite by cold compression and hot sintering technology. Besides that, such ceramic substance is shown to have reliability and economical efficiency and suitable for large-scale production of salt based composite. This work also employs a carbon enhancer of natural graphite power as TCA to promote the thermal conductivity of the salt composite. More specifically, the optimal composition among the ingredients of quinary salt, HNT and graphite was first evaluated by conducting leakage visualization inspection on different formulations of composites. A sequence of measurements was then carried out to investigate the microstructural characterization, chemical and thermal stability, phase change behaviour and thermal conductivity of the composite. Finally, the composite cycling performance was determined by analysing the composite chemical structure and thermal properties during the repeated heating and cooling cycles. The results indicated that the quinary salt-HNT-graphite composite with considerably low phase transition temperature and an outstanding combination of thermal properties and cycling performance could be an effective candidate instead of traditional organics used in low temperature thermal energy storage fields.

2. Materials and methods

2.1. Raw materials

A eutectic quinary nitrate salt is used as PCM in this work, which is consisted of $NaNO_3$, $NaNO_2$, KNO_3, KNO_2 and $LiNO_3$. All these single salts are of analytical grade and got from Bejing Yili Fine Chemicals Co., Ltd, China. A hallyosite nanotube with a purity of 95% is purchased from Jiangsu Xianfeng Nanomaterials Technology Co., Ltd, China, and employed as SSM. Natural graphite power is used as thermal conductivity enhancer, which has a predominant particle size of 3-5 μm

and is got from Beijing Jiashiteng Co., Ltd, China. All raw materials are utilized as received with no further treatment.

2.2. Preparation of quinary nitrate salt

A static melting approach is used for the eutectic quinary salt preparation [10]. Specifically, the single salts of KNO_2, $NaNO_2$, KNO_3, $NaNO_3$ and $LiNO_3$ are first dried in an electro-thermostatic blast oven (101-3AB, Tianjin TAISITE Instruments Co., Ltd, China) at 100 °C for 12 h to remove the moisture, followed by weighing the salts in a balance according to a desired mass ratio of 51.58:15.56:1.58:1.33:29.95. The samples are then adequately mixed to achieve uniform mixing in a ball grinder, and heated in a muffle furnace (KJ-M1200-12LZ, Zhengzhou Kejia Electric Furnace Co., Ltd, China) with the use of following temperature program: starting heat from room temperature to 150 °C at 10 °C/min, and holding at 150 °C for 0.5 h; heating further at a rate of 5 °C/min to 400 °C, and maintaining at 400 °C for 12 h. After the mixed salts are fully melted, a reversed temperature program to the heating process is used to cool the sample to environment temperature. Finally, the molten mixture is taken out from the furnace and milled in a high-efficient pulverizer to obtain the eutectic salt power. The milled quinary nitrates are stored in a thermotank for further experiments.

2.3. Preparation of quinary salt based composite

The quinary nitrate salt composite is fabricated with the use of a so-called cold compression and hot sintering approach and the process is illustrated in Fig. 1. The detailed procedure involves the following three steps. Firstly, an anticipant mass ratio of the salt, HNT and graphite is accurately weighed and equably mixed in a ball grinding mill for 2 h with a speed of 250 rpm to realize even mixing. Secondly, the mixed powder is shaped and compressed into disk-like configuration in a self-designed stainless steel mould by using a pressure of 80 MPa to get a dimension size of 12.5 mm in diameter and 8 mm in thickness. Lastly, the green pellet is calcined in a muffle furnace based on the following temperature routine: sintering from ambient temperature to 100 °C at a rate of 5 °C/min, and sustaining at 100 °C for 0.5 h; sintering further at the same rate from 100 °C to 200 °C, and maintaining such a temperature for another 1 h; and finally cooling the sample to ambient temperature with a backward process to the heating programme. The sintered composite obtained from the above processes is kept into a thermotank for further test and characterization. Repeating the fabrication procedure and altering the concentration of the ingredients, various composites can be achieved.

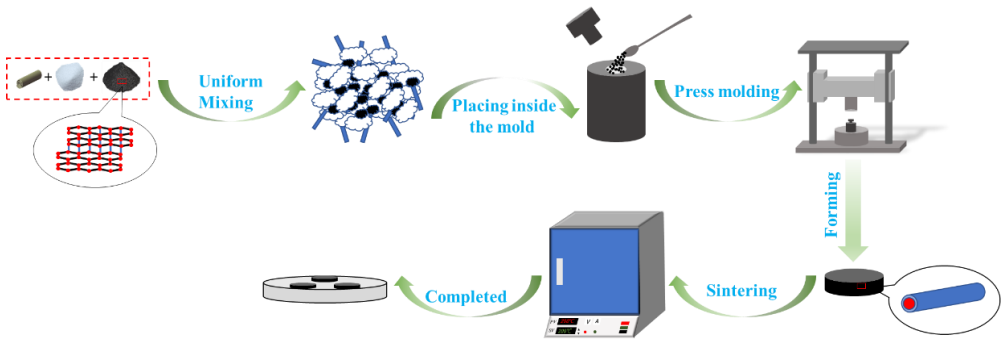

Fig. 1. Schematic diagram of the fabrication process for the quinary salt based composite.

2.4. Characterization of composites

The microstructure characteristics of the composite are observed by using a Scanning Electron Microscope integrated with an Energy Dispersive Spectrometer (SEM-EDS, HITACHI SU9000, Japan). The chemical structure and compatibility of the composite are measured with the use of an X-ray diffraction (XRD, BURKER D8 ADVANCE, UK) with a scanning angle over 10-90° and a step interval of 0.02°, and also a Fourier transformation infrared spectroscope (FT-IR, B420, SpectrumII, US) with the spectrum from 400-4000 cm^{-1}. The composite thermophysical properties involving the melting point, latent heat and specific heat are analysed by a Differential Scanning Calorimeter (DSC, 214Polyma, NETZSCH, Germany). A thermogravimetric analyser (TG, 209F1 Libra, NETZSCH, Germany) and a Laser Flash Analyser (LFA 457, NETZSCH, Germany) are respectively employed to measure the composite thermal stability and thermal conductivity. A self-built facility containing both a high temperature chamber and a low temperature chamber is used to evaluate the cycling performance of the composite. A heating and cooling rate of 5 °C/min is selected for experiments, and a thermocouple inserted into the composite is used for monitor the composite temperature and control the thermal cycling.

3. Results and discussions

3.1. Confirmation of optimal composition in the composite

As mentioned above, various composites can be obtained by altering the ingredient concentration of salt and HNT based on the hot sintering fabrication approach. The decent selection of HNT concentration can not only achieve the composite stable structure to avoid the liquid leakage during phase transition process, but also endow the composite with high energy storage ability. Therefore, the optimal composition in the composite has been checked and confirmed prior to the further experiments. For doing so, eight sets of samples containing different mass ratios of HNT with a range of 20-80 wt.% are prepared and investigated. Fig. 2 shows the photographs of these samples before and after sintering. In the figure, the labels of C8-C1 respectively correspond to the composites with HNT mass concentrations of 20-80 wt.%. The detailed results on the visual inspection on these samples are tabulated in Table 1. It can be seen that there is existence of apparent liquid leakage and structure distortion when the HNT concentration is less than 40 wt.%. For the sample containing 45 wt.% HNT, slight salt leakage is observed in the material outer surfaces and no obvious shape deformation is occurred. In the case of HNT loading higher than 50 wt.%, excellent appearance with no deformation and leakage is found in the composite. These observations indicate that for achieving the structure stabilization of the composite and eliminating the salt leakage, at least 50 wt.% of HNT is required over the fabrication process. Namely, case C4 is regarded as the optimum formula and hence is further chosen to mix with graphite for thermal conductivity enhancement. As shown in Fig. 2 (c) and (d), which gives the pictures of composite with different concentration of graphite before and after sintering. One can see that for a given graphite concentration of 2-10 wt.%, all composites present consummate appearance and stable structure. This indicates that 50 wt.% of HNT endows with the composite ability to retain 10 wt.% graphite without the happening of salt leakage and distortion.

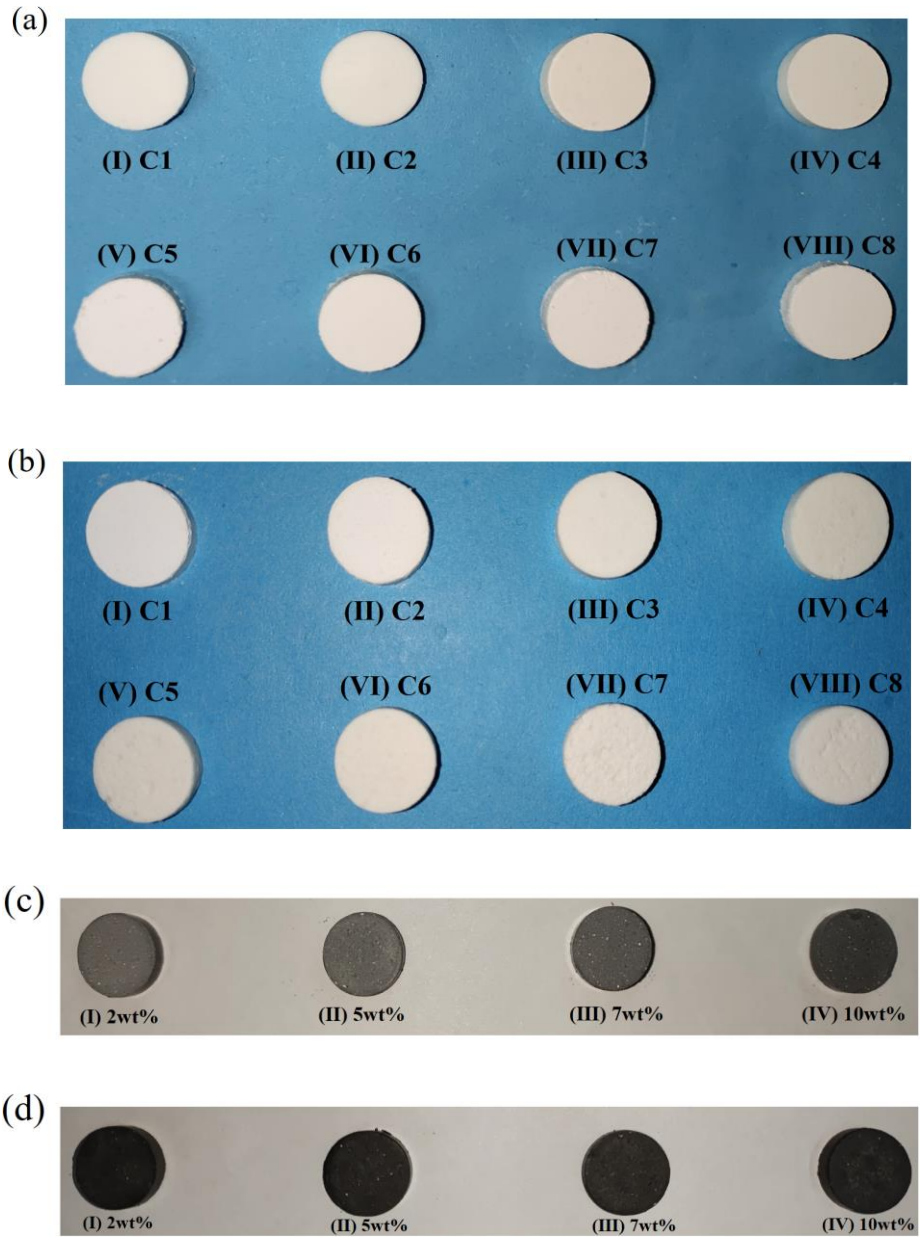

Fig. 2. Photographs of the composites. (a) samples without graphite before sintering, (b) samples without graphite after sintering, (c) samples with graphite before sintering, and (d) samples with graphite after sintering.

Table 1. Different fabrication cases for the composites and visual inspection after sintering.

Samples	C1	C2	C3	C4	C5	C6	C7	C8
Salt (wt.%)	20	30	40	50	55	60	70	80
HNT (wt.%)	80	70	60	50	45	40	30	20
Graphite (wt.%)	~2-10 (*)							
Intuitive form (Δ)	a	a	a	a	b	c	c	c

(*): the graphite accounts for the ratio of the total mass of the salt-HNT composite; (Δ) a indicates

that the composite has a stable structural morphology after sintering and no collapse; b indicates slight liquid leakage of the composite after sintering; c indicates serious structural deformation and leakage in the composite after sintering.

3.2. Microstructural characterization of the composite

Fig. 3 shows the SEM images of HNT and the composite containing a ratio of salt:HNT:graphite=5:5:1 after sintering. It can be seen that for HNT, a clear hollow tubular structure with a diameter range of 60-100 nm and a length range of 200-1500 nm is observed, as illustrated in Fig. 3 (a). Such distinctive feature could be able to provide extra contact surface area to encapsulate salt and thereby effectively restrain the liquid leakage during the phase transition process. As for the salt based composite, a reasonably homogeneous distribution of salt and other two ingredients is observed in the detection area after experienced mixing and sintering processes (Fig. 3 (a)). From Fig. 3 (c) and (d), it can also be seen the formation of a distinct molten salt liquefied structure. This structure plays a significant role in maintaining the ceramic and graphite substances together and sustaining the structural stability. Our previous investigations have demonstrated the structure formation mechanism of the salt based composite [21, 22]. For the salt composite prepared in this work, the physical blending and geometry shaping enable a homogeneous distribution of the three ingredients, and an increase in the density within the composite over the green sample fabrication process. During sintering, the salt melts and changes the state when the temperature is over the melting point. In such a process, the microscaled movement of liquid salt in the confined area occurs to form the molten salt liquefied structure, which pull the migration of skeleton substance moving together and lead to the occurrence of particle rearrangement within the composite. Due to the high wettability of skeleton ceramic towards the salt, the liquid salt can be efficaciously encapsulated by the ceramic material and accommodated within the composite. In the meantime, the swelling impact caused by the low surface energy of graphite towards the salt can also be overcome, permitting the formation of a compact and dense composite.

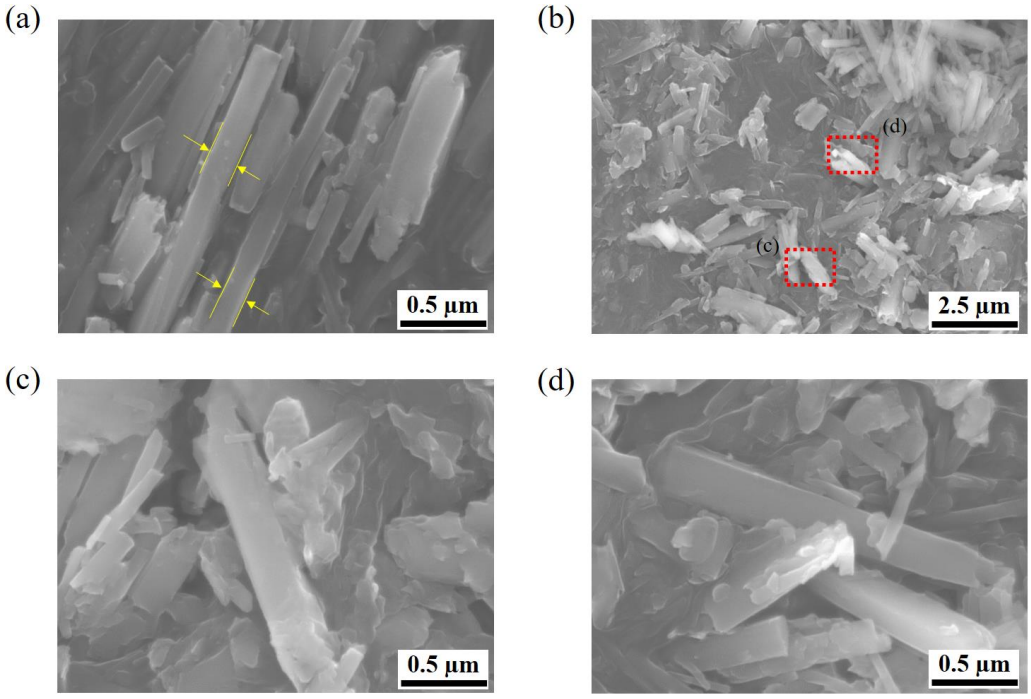

Fig. 3. (a) SEM image of HNT; (b) SEM image of the composite with a ratio of salt:HNT:graphite=5:5:1 after sintering; (c) Capture SEM image from the rectangular area of Fig. (b); (d) Capture SEM image from the rectangular area of Fig. (b).

Fig. 4 illustrates EDS element distributions in the composite after sintering. The mapping analyses are performed by identifying the distributions of Si, Al, Na and K elements. The former two elements are used to indicate the HNT, while the latter two are employed to stand for the quinary salt. These elements are believed to be sufficient to express the distributions of HNT and salt in the composite. From Fig. 4, one can see that all elements are pretty well distributed in the observation area with the element of Na and K completely filled the voids that formed by Si and Al. Such observation further denotes that a homogeneous distribution of particles has been achieved in the composite. This phenomenon can be interpreted as follows. For a form-stable composite containing salt as PCM, the high-temperature sintering leads to the occurrence of salt phase transition from eutectic state to viscous liquid. During such a process, the motion of liquid salt within the micro-pores occurs, pulling the ceramic particles movement together to form liquid bridges because of the high surface energy of ceramics towards to salt. This migration of salt causes the rearrangement and redistribution of HNT and graphite, allowing the uniform distribution of ingredients in the composite after sintering.

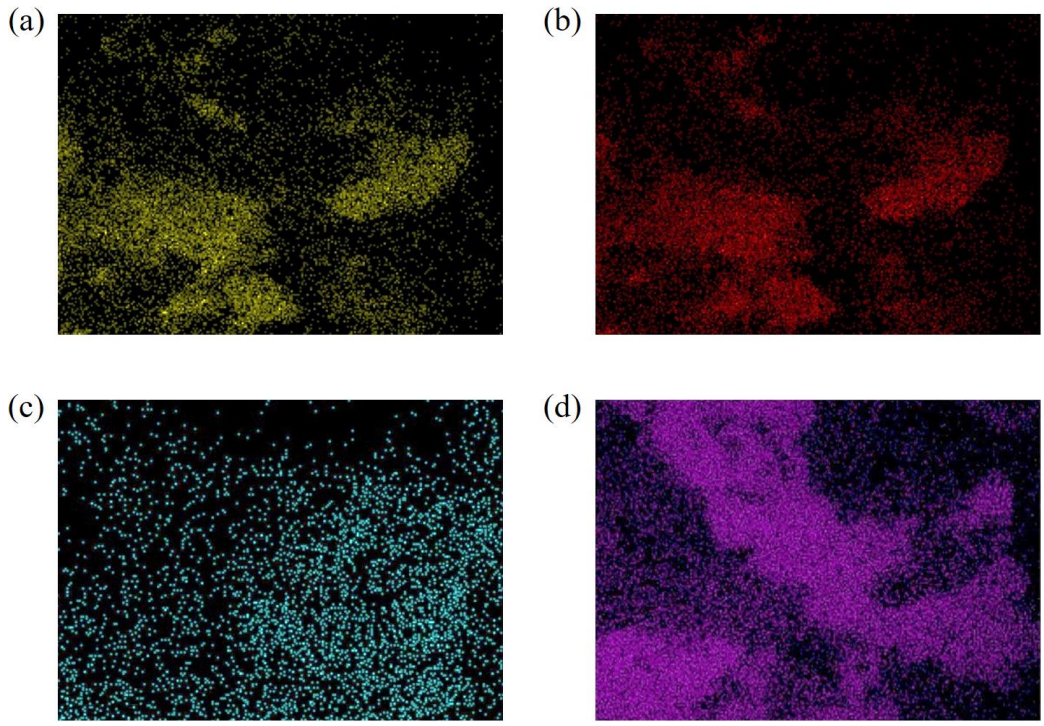

Fig. 4. EDS element maps of Si (a), Al (b), Na (c) and K (d) in the composite.

3.3. Chemical and physical compatibility of the composite

Fig. 5 plots the XRD patterns of the salt based composite. For comparison, the results for pure quinary salt, HNT and graphite are also included in the figure. It can be seen that nine major peaks at 2θ=12.0°, 19.1°, 23.7°, 30.5°, 32.2°, 33.8°, 41.3°, 44.5° and 62.2° are apparent in the salt-HNT composite after sintering, as demonstrated in Fig. 5 (d). This is similar with the peaks appeared in the pure quinary salt and HNT (Fig. 5 (a) and (b)), denoting good chemical compatibility between the salt and HNT. Fig. 5 (c) illustrates the XRD analysis for natural graphite, and it is seen that a distinct peak of 26.3° and a misty peak of 54.4° are observed, which is in agreement with the observations reported by reference [23]. For the salt-HNT composite containing graphite, as indicated in Fig. 5 (e), the XRD pattern only contains the peaks of salt/HNT composite and graphite, and no new peak is emerged, indicating that there are no chemical reactions happened among the ingredients of quinary salt, HNT and graphite, and a splendid chemical compatibility is reached within the salt composite.

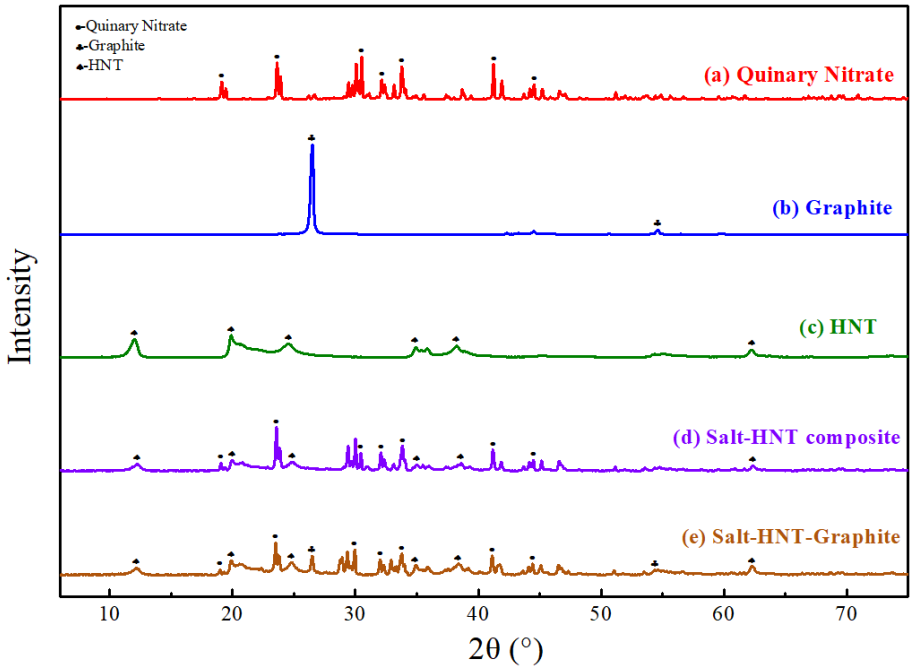

Fig. 5. XRD patterns of the (a) quinary salt, (b) HNT, (c) graphite, (d) salt-HNT composite, and (e) salt-HNT-graphite composite.

To further determine the chemical and physical compatibility of the salt-HNT composite, the FT-IR analysis is also carried out. Fig. 6 illustrates the measurement results. One can see that for quinary salt, three main spectrum peaks of 830 cm^{-1}, 1270 cm^{-1} and 1650 cm^{-1} are distinct, as plotted in Fig. 6 (a). These observations are mainly due to the in-plane flexural vibration of NO_3^{-1}, stretching vibration of NO_2^{-1}, and antisymmetric stretching vibration of NO_3^{-1}. For HNT, there are five peaks appearing at 459 cm^{-1}, 535 cm^{-1}, 1095 cm^{-1}, 3623 cm^{-1} and 3699 cm^{-1} (Fig. 6 (b)). The first peak is induced by the Al-O-Si deformation vibration, and the latter four peaks are respectively assigned to Si-O-Si stretching vibration, Al-OH stretching bands, apical Si-O stretching and Al-OH bending band [24, 25]. Mixing of quinary salt and HNT to fabricate composite has no impact on the material stability where no new characteristic peaks are found, as shown in Fig. 6 (d). For graphite, it is noticed that two obvious peaks of 1635 cm^{-1} and 3441 cm^{-1} are apparent (Fig. 6 (c)). The peak of 1635 cm^{-1} is induced by the C=C stretching, and the peak of 3441 cm^{-1} can be attributed the stretching vibration peak of -OH bond that induced by residual water in the sample. The addition of graphite into the salt-HNT composite has not been caused the chemical reaction in the composite and the same absorption peaks as these exhibited in the ingredients of quinary salt, HNT and graphite have been observed, indicating that all components are chemically compatible. These results combined with the observations shown in Fig. 5 denote that the salt based composite developed in this work achieves a preeminent chemical stability and compatibility.

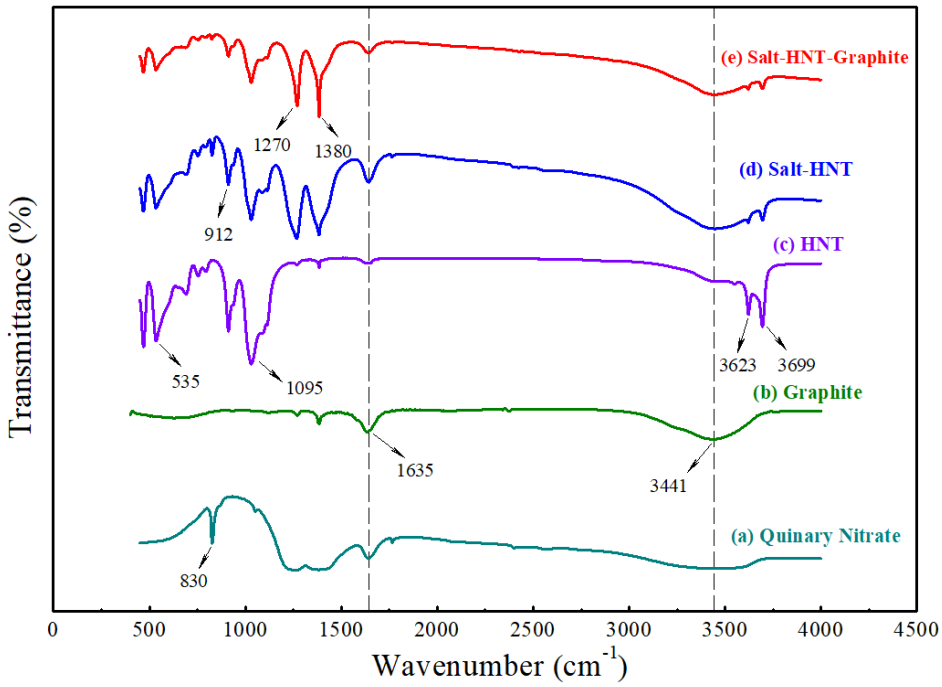

Fig. 6. FT-IR spectra of the (a) quinary salt, (b) HNT, (c) graphite, (d) salt-HNT composite, and (e) salt-HNT-graphite composite.

3.4. Thermophysical properties of the composite

3.4.1. Phase change behaviour of the composite

The phase change behaviours of the salt based composite are evaluated by DSC. Fig. 7 plots the results, in which the measured data for melting temperature and latent heat as well as heat capacity are involved. It can be seen that since there is no chemical reaction occurred in the composite, only one endothermal peak is observed for both the pure quinary salt and composite at the temperature range of 30-200 ℃. For the convenience of analysing, only the measured curves at a temperature of 50-110 ℃ are depicted in the figure. Table 2 summarises the detailed results. One can see that the pure quinary salt achieves a quite low melting temperature with the onset and peak values being respectively measured as 72.51 ℃ and 78.41 ℃. The peak melting points of the salt-HNT composite and salt-HNT-graphite composite are respectively 78.3 ℃ and 78.4 ℃, which corresponds closely to that of the pure quinary salt. These results reveal that the developed composite with a considerably suitable low phase change temperature can be an effective alternative for replacement of organics used in low temperature fields. The measured latent heat for the pure quinary salt is determined as 135.46 kJ/kg. The addition of HNT triggers a decline in latent heat of the composite, and the value is decreased to 67.68 kJ/kg when 50 wt.% HNT is contained. The involvement of graphite gives a further reduction in the composite latent heat. Generally, the theoretical latent heat in a salt based composite should be linearly proportional to the concentration of the salt, and it can be calculated by the following expression:

$$\Delta H = \delta \Delta H_{salt} \quad (1)$$

where ΔH is the composite latent heat, δ is the salt mass ratio within the composite, and ΔH_{salt} is the salt latent heat. For the composite illustrated in Table 2, the measured latent heat value is in close proximity to the theoretical one with slight deviation less than 0.5% existed. This is mainly due to the incomplete encapsulation of salt at the composite surface, which results in the divulgence during the phase change process and hence the reduction of measured value for material latent heat. But nonetheless, this observation further indicates the excellent chemical stability among the components of salt, HNT and graphite. From Table 2 it is also seen that the melting temperature of the composite is lower than that of the pure quinary salt. The penetration of salt into the hollow tubular of HNT could be a reason for this reduction. Another reason could be attributed to the change of entropy [23]. For a salt based composite, the entropy value of salt within the composite is typically larger than that of the salt in pure state. Therefore, the composite phase transition point will be lower than that the pure salt under a stable melting or solidifying condition.

Involved in Table 2 also are the heat storage density of the salt composite. For convenient calculation, the heat capacities of the ingredients of pure salt, HNT and graphite are measured and tabulated in the table. The total heat storage capacity of a salt composite can be calculated according to the following formula [26]:

$$Q_e = (1-\eta)\int_{T_s}^{T_e} c_{p,csm}dT + \varphi\int_{T_s}^{T_e} c_{p,tce}dT + \eta\left(\int_{T_s}^{T_m} c_{ps,pcm}dT + \Delta L_m + \int_{T_m}^{T_e} c_{pl,pcm}dT\right) \quad (3)$$

where Q_e stands for the energy storage density of the composite, T_s and T_e respectively denote the starting and end temperatures, c_p is the heat capacity, η and φ are respectively the mass ratio of the HNT and graphite within the composite, ΔL_m is the latent heat of quinary salt. It is seen from the table that the heat capacities of the HNT and graphite are respectively measured as 0.514 kJ/kg · ℃ and 0.710 kJ/kg · ℃, which are smaller than the pure quinary salt where a measured value of 1.29 kJ/kg · ℃ is obtained. Based on the heat capacity values, the composite heat storage density can be obtained. As shown in the table, the heat storage capacity of the composite containing either 10 wt.% or not is reached up to 497 kJ/kg at a temperature range of 25-510 ℃. Such value is significantly higher than some conventional organics and hydrate salts, and hence has the edge on the competition to be utilized in low temperature thermal energy storage fields.

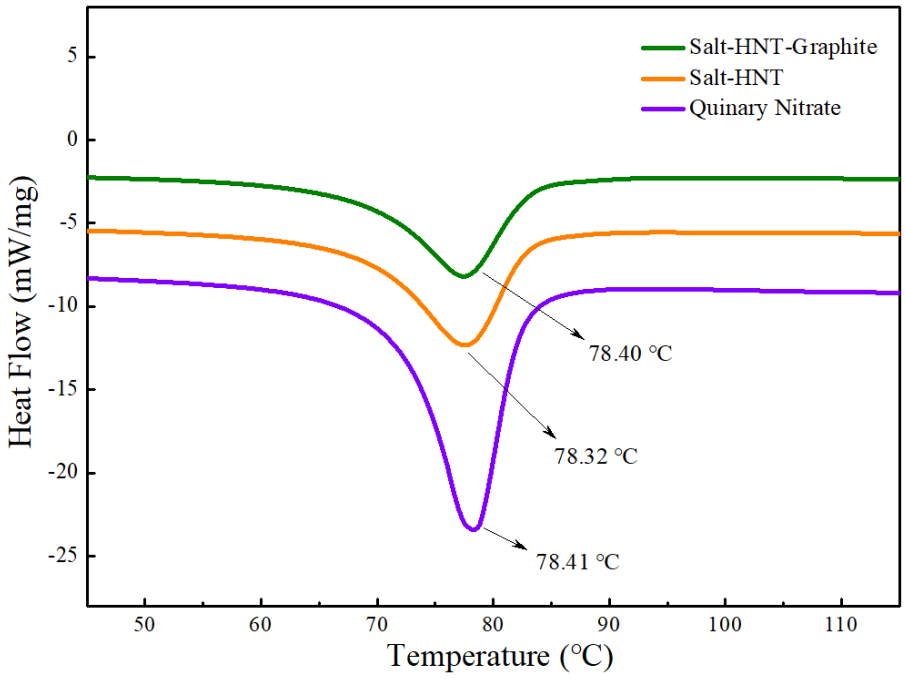

Fig. 7. DSC curves of the pure quinary salt, salt-HNT composite and salt-HNT-graphite composite.

Table 2. DSC measurements for the pure quinary salt, HNT, graphite and the composite.

Name	Onset (°C)	Peak (°C)	Endset (°C)	Specific Heat (J/g · °C)	Latent Heat (J/g)	Energy storage density (J/g, 25-510 °C)
Salt	72.51	78.41	83.07	1.290	135.46	761.11
HNTs	-	-	-	0.514	-	-
Graphite	-	-	-	0.710	-	-
Salt-HNT	72.50	78.32	83.01	0.880	67.68	494.48
Salt-HNT-Graphite	72.47	78.40	82.96	0.894	64.35	497.94

3.4.2. Thermal stability of the composite

In order to evaluate the maximum allowable operation temperature and also the effect of using HNT as skeleton supporting material on the composite thermal stability, the thermogravimetric analyses are carried out under an air environment and the results are plotted in Fig. 8. For comparison, the result for pure HNT is also involved in the figure. It can be seen that for pure quinary salt, a one-step degradation in the weight loss is observed in which the sample starts to lose weight from 490 °C. In general, the decomposition temperature of a tested sample can be regarded as the moment where over 3% of initial weight has been lost during the TGA measurement [26]. Therefore, the thermal decomposition temperature of the quinary salt can be measured as 512 °C. When the HNT is added into the quinary salt to fabricate composite, the thermal decomposition curve becomes more

complex in which a two-step degradation is apparent. Such observation can be attributed to the physical characteristics of HNT. As illustrated in the insert of Fig. 8, the thermal decomposition of HNT experiences an obvious three-step process: the step one is the normal temperature section; the step two takes place at a temperature of 300 ℃ and is a water loss stage in which the complete transformation of the layer spacing from 10Å to 7Å is occurred; the step three is the dehydroxylation stage when the temperature is around 500 ℃. The thermal decomposition of the composite combines the weight loss characteristics of pure salt and HNT, and hence presents two distinguishable degradations, as shown in Fig. 8. The maximum decomposition temperature can be determined as 530 °C, which is higher than that of quinary salt. This confirms that the HNT can be served as supporting matrix to improve the thermal stability of the quinary salt. An explanation for such observation could be as follows. In a salt-HNT composite, the hollow tubular structure of HNT provides enlarged surface to absorb and encapsulate salt. Meanwhile, the untreated HNT contains residual water on the interlayer and surface, as exhibited in weight loss curve in Fig. 8. When the operating temperature is increased from 25 °C to 650 °C, the HNT releases water first and then occurs the dehydroxylation at a temperature of 500 ℃. During such a process, a change in the crystal structure is happened, leading to the enlargement of lumen of HNT [27, 28]. Fig. 9 illustrates the thermal weight loss process of a salt based composite containing HNT. It can be inferred that the microstructure change of HNT offers extra space to accommodate the molten salt and prevent it from decomposing.

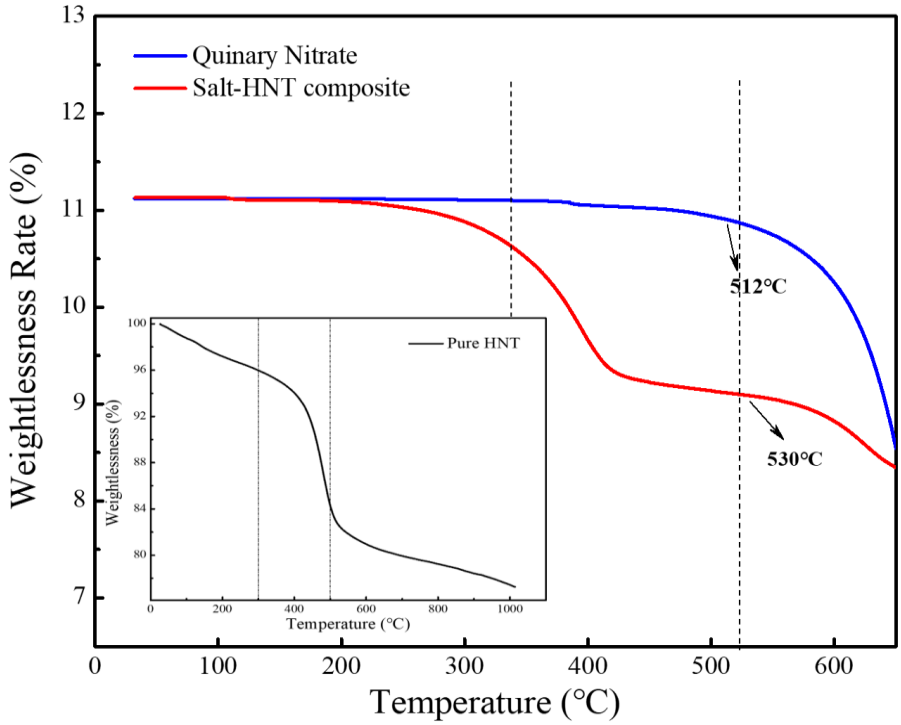

Fig. 8. TGA curves of the quinary salt and salt based composite; the insert is TGA result for HNT.

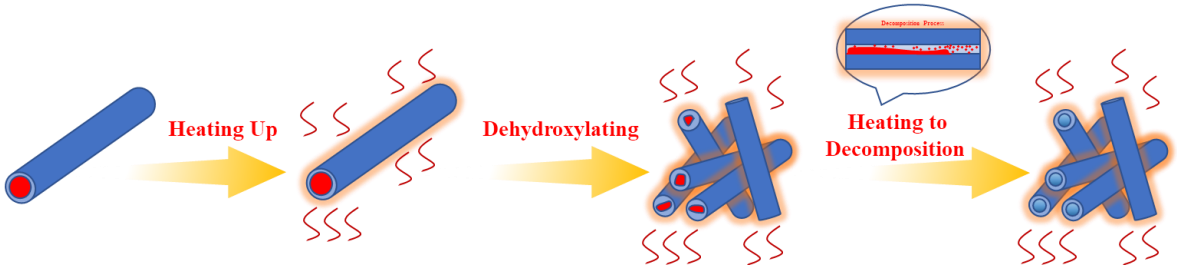

Fig. 9. Schematic diagram of the thermal weight loss process of composite containing HNT.

As discussed in the last section, two major advantages of the salt composite developed in this study are its low phase change temperature and high thermal decomposition temperature, which offers the composite spacious temperature range that could be able to utilize in some special thermal energy storage scenarios such as building energy conservation and industrial waste heat recovery where a large temperature fluctuation is existed. To verify the superiority of the present salt based composite, several typical materials investigated in the literatures that have similar melting temperatures to the quinary salt are compared and the results are summarised in Table 3. One can see that the developed composite exhibits not only the largest temperature range but also the reasonably lowest melting temperature among the selection materials. The temperature range mentioned here stands for the distinction between the melting temperature and decomposition temperature. A wide temperature range denotes that the material has great ability to bear the risk of decomposition in real applications. As shown in Table 3, the composite temperature range is reached up to 460 °C on the premise of melting point around 75 °C, which is nearly 2.5 times higher than that of the paraffin based materials, two and three times higher than the hydrated salt and polyethylene glycol. This result indicates that the present quinary salt based composite could be able to serve as a promising candidate to substitute organic substances utilized in low and middle temperature applications.

Table 3 Comparison of thermophysical properties of the composite fabricated in this work with other typical materials.

CPCMs	Onset (°C)	Peak (°C)	Endset (°C)	ΔH (J/g)	Tg (°C)	ΔT (°C)	λ (W/m·K)	Refs.
SA/TATP-TAPA	63.0	71.9	93.8	136.8	-	-	0.4215	[29]
PA/CPS	-	65.7	-	95.5	-	-	-	[30]
SA/CNT@PC	-	70.7	-	155.7	200	129.3	1.023	[31]
PEG/BN/chitosan	64.6	-	-	136.9	200	135.4	2.77	[32]
PEG/GNP-melamine	-	61.7	-	178.9	-	-	0.26	[33]
n-octacosane/Cellulose/ CNTs	-	68.5	-	252.9	311.2	242.7	0.58	[34]
SA/Co_3O_4/EG-10	-	69.44	-	192.47	259	189.56	2.53	[35]
n-alkane/Cellulose nanofiber/ black phosphorus	-	66.0	-	251.6	324.2	258.2	0.448	[6]

PW/CF-1300	47.5	66.5	73.1	221.1	200	152.5	-	[36]
Diatomite/PEG/silver nanowire	59.83	-	-	110.7	367	307.17	0.82	[7]
SA/BN/EG-12	67.85	-	-	153.75	200	132.15	6.349	[8]
PEG/GO/GNP	59.0	65.5	72.1	185.7	-	-	1.43	[37]
PEG/MPMF	54.5	62.5	75.5	186.2	392.6	338.1	-	[10]
Present sample	72.47	78.40	82.96	64.35	530	457.53	1.31	

3.4.3. Thermal conductivity of the composite

It has been broadly reported that the effective thermal conductivity of the composite can be largely enhanced through the addition of carbon additives [21, 22]. In this work, the graphite is used as TCA for composite fabrication and its effect on the composite thermal conductivity is investigated in this section. Fig. 10 shows the measured results under an operating temperature of 25 °C. One can see that the composite thermal conductivity is increased with increasing the graphite concentration. In the case of the composite with no graphite addition, the thermal conductivity is measured to be 0.621 W/m·K, which is increased to 1.315 W/m·K when the graphite concentration is 10 wt.%. Compared to other substances that owning similar phase transition temperature below 100 °C, as summarized in Table 3, the thermal conductivity of the salt composite developed in this work is nearly 2-5 times higher than the paraffin and hydrated salt composite. Also shown in Fig. 10 is the fitting curve for the measurement results of the composite thermal conductivity. It is seen that for a given graphite loading range of 0-10 wt.%, the composite thermal conductivity can be identified as linearly proportional to the graphite content. A close check of Fig. 10 also finds that the thermal conductivity of the composite containing no graphite is higher than the pure quinary salt. For nitrate salts, the average thermal conductivity is around 0.5 W/m·K [19], while the thermal conductivity of the salt-HNT composite is determined as 0.62 W/m·K. This result indicates that the employment of HNT as skeleton material has improved the thermal conductivity of the quinary salt. The main cause for this observation lies in the unique tubular structure of the HNT, which is beneficial to the formation of conductive network and thereby the improvement of effective thermal conductivity in the salt composite.

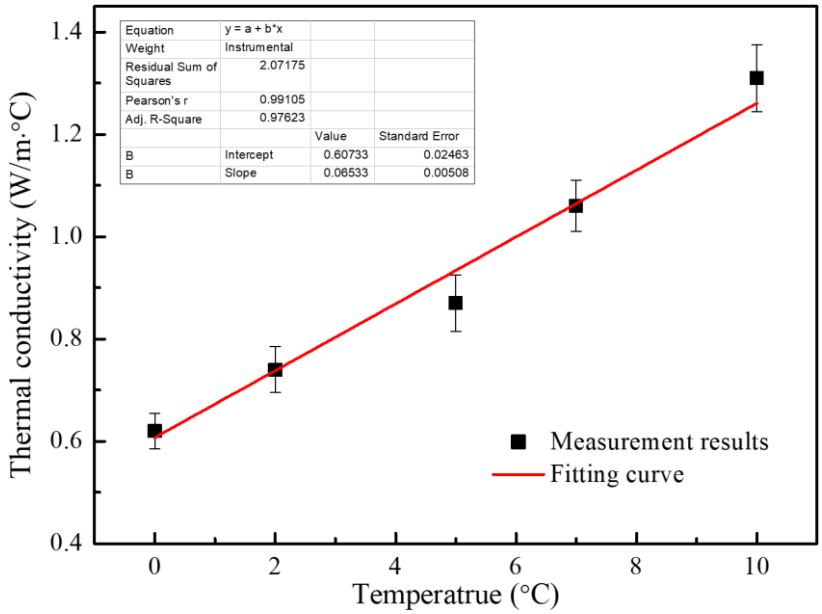

Fig. 10. Thermal conductivity of the composite containing different mass loading of graphite.

Fig. 11 shows the relationship between the thermal conductivity and operation temperature. It can be seen that for a selected temperature range of 25-200 °C, there is an inflection point on experimental data apparent during which the thermal conductivity first decreases with temperature from 25 °C to 70 °C, then reaches a minimum value at a temperature of 70-85 °C and finally increases with temperature up to 200 °C. Similar trend on thermal conductivity measurement has also been observed by Yang et al. [38] and Anagnostopoulos et al. [39]. The reason for this observation can be explained as follows. In an insulating sample, the heat is principally transmitted by the pattern of lattice vibration or phonons due to the inconspicuous impact of free electrons to conduction. In such circumstance, the thermal conductivity of the substance is mainly related to the heat capacity, and phonons mean free path velocity. Consequently, the measured thermal conductivity is found to decrease with temperature in the case of operation temperature is higher than the Debye temperature. But in spite of this, the composite thermal conductivity measurement at the working temperature range is difficult and detailed explanation remains to be further explored.

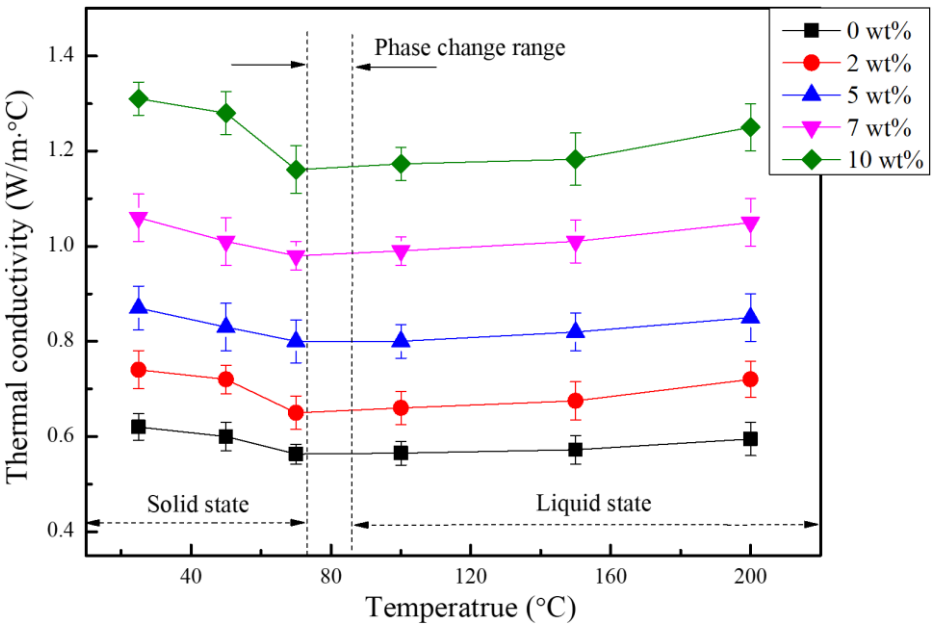

Fig. 11. Measured thermal conductivity of the composites versus temperature and graphite loading.

3.5. Thermal cycling performance of the composite

The thermal cycling performance of the composite is evaluated in this section. For doing so, the XRD and FTIR as well as DSC analyses are performed to check the behaviour of the composite that experienced different heating-cooling cycles. Fig. 12 illustrates the crystal structure and infrared spectrum of the salt based composite went through different heating-cooling cycles. It can be seen that all characteristic peaks in the samples after 50, 100 and 400 thermal cycles are identical to these observed in the individual materials of quinary salt, HNT and graphite, as well as the composite experienced one thermal cycle. This further demonstrates no new chemical bond created in the composite at elevate temperatures, and an outstanding physical and chemical stability over the repeated thermal cycles. Fig. 13 shows the DSC comparison results. It can be seen that three similar endothermal curves are observed for all measured samples. After experienced 400 times of heating-cooling cycles, the phase transition behaviour of the composite change very little with the phase change point and latent heat respectively being measured as around 72.5 °C and 64 kJ/kg. The variation of phase change point may be attributed to the salt encapsulation and movement in the micropores formed by the tubular structure of HNT, while the slight reduction of the measured latent heat is mainly due to the divulgence of salt in the heating-cooling cycle process. In a salt-HNT composite, the incomplete accommodation of quinary salt at the outer surface could occur the spillage and hence leads to the decrease of the latent heat. It is worth pointing out that although the latent heat of the developed composite is not very high (only around 65 kJ/kg) and the use of such composite in real applications seems to be a challenge, the large temperature range gives the composite the ability to be a competitive candidate utilized in low and medium thermal energy storage particularly in the situation where there exists a large fluctuation of temperature and the traditional low temperature PCMs is powerless. This results together with the observations obtained from Fig. 12 reveal that the quinary salt based composite fabricated in this work has achieved an

excellent stability and long-term reliability that propitious for low and medium thermal energy storage applications.

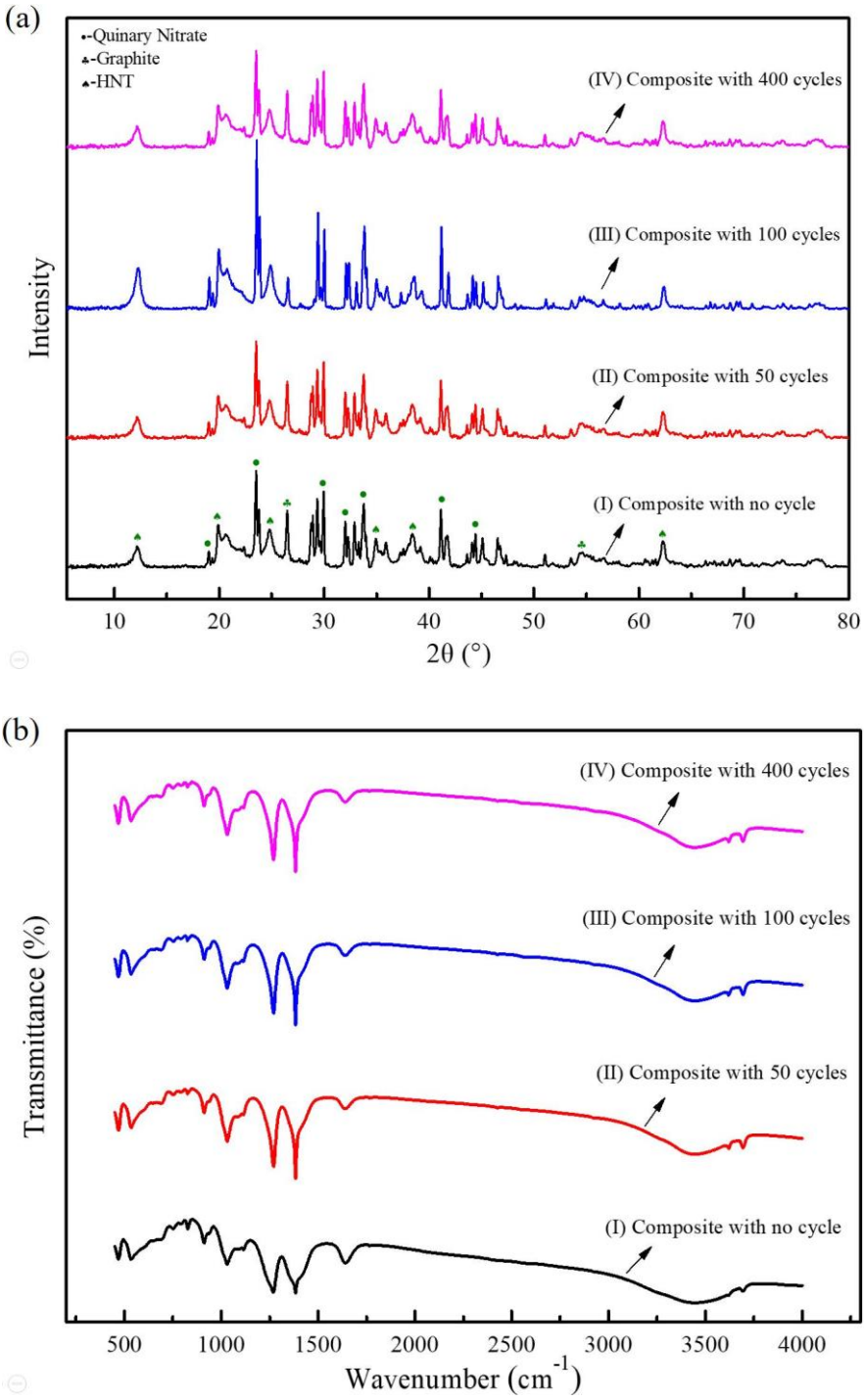

Fig. 12. Thermal cycling stability of the composite experienced different times of heating and cooling cycles. (a) XRD and (b) FTIR measurements.

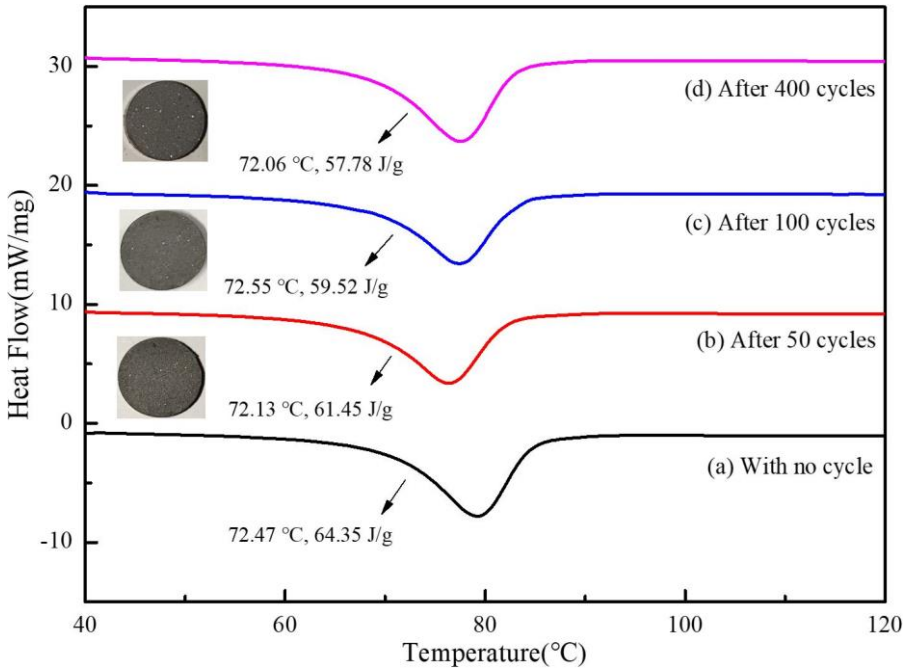

Fig. 13. DSC measurements of the composite experienced different times of heating and cooling cycles.

3. Conclusions

A quinary salt-HNT-graphite composite was developed and investigated in this work. The optimal composition among the ingredients of quinary salt, HNT and graphite within the composite was first evaluated by conducting leakage visualization inspection. A variety of measurements were then carried out to investigate the microstructural characterization, chemical and thermal stability, phase change behaviour and thermal conductivity of the composite. Finally, the composite cycling performance was determined by analysing the composite chemical structure and thermal properties during the repeated heating and cooling cycles. The following conclusions can be obtained according to the investigations:

(1) The hollow tubular structure of HNT could be able to provide extra contact surface area to accommodate quinary salt within the composite and thereby effectively eliminate the liquid leakage during the phase change process.

(2) The addition of HNT and graphite into quinary salt has not caused the chemical reaction in the composite, indicating preeminent chemical stability and compatibility has been achieved in the composite.

(3) A mass fraction of 50 wt.% HNT endows the composite with the optimal formulation in which 10 wt.% graphite can be successfully accommodated and a thermal conductivity of 1.31 W/m·K can be acquired. In such a composition, the composite presents a considerably low melting temperature of 72.4 °C and a high thermal decomposition temperature of 530 °C. This spacious temperature difference achieves the composite a large heat storage density over 500 kJ/kg at a temperature range of 25-510 °C.

(4) The composite achieves splendid stability and long-term reliability that could be an effective candidate to substitute traditional organic materials utilized in low and medium temperature thermal energy storage fields.

This work concerns only the development of a novel low temperature quinary nitrate salt based composite phase change material with the use of HNT as skeleton supporting material. Investigation of system efficiency and performance enhancement by utilizing such a salt composite is beyond the scope of this work but it is worth exploring nevertheless in the future.

Acknowledgements

The work was supported by the Beijing Natural Science Foundation (3222026), and high-end talents development program, Carbon Neutral Foundation (049000514122611) and International Research Cooperation Seed Fund (Project No. 2021B40) of Beijing University of Technology.

References

[1] Ekaterina Pomerantseva, Francesco Bonaccorso, Xinliang Feng, Yi Cui, Yury Gogotsi. Energy storage: The future enabled by nanomaterials. Science 366 (2019) 6468.

[2] Fan-Yi Meng, I-Han Chen, Jiun-Yi Shen, Kai-Hsin Chang, Tai-Che Chou, Yi-An Chen, Yi-Ting Chen, Chi-Lin Chen, Pi-Tai Chou. A new approach exploiting thermally activated delayed fluorescence molecules to optimize solar thermal energy storage. Nature Communications 13 (2022) 797.

[3] Jason Woods, Allison Mahvi, Anurag Goyal, Eric Kozoubal, Adewale Odukomaiya, Roderick Jackson. Rate capability and Ragone plots for phase change thermal energy storage. Nature Energy 6 (2021) 295-302.

[4] Juan Wei, Chenyuan Liu, Jiayu Duan, Aiwen Shao, Jinlu Li, Jiangang Li, Wenjie Gu, Zixian Li, Shujuan Liu, Yun Ma, Wei Huang, Qiang Zhao. Conformation-dependent dynamic organic phosphorescence through thermal energy driven molecular rotations. Nature Communications 14 (2023) 627.

[5] A. Lyden, C.S. Brown, I. Kolo, G. Falcone, D. Friedrich. Seasonal thermal energy storage in smart energy systems: District-level applications and modelling approaches. Renewable and Sustainable Energy Reviews 167 (2022) 112760.

[6] Xiaosheng Du, Jinghong Qiu, Sha Deng, Zongliang Du, Xu Cheng, Haibo Wang. Flame-retardant and form-stable phase change composites based on black phosphorus nanosheets/cellulose nanofiber aerogels with extremely high energy storage density and superior solar-thermal conversion efficiency. Journal of Materials Chemistry A 8 2020 14126-14134.

[7] Tingting Qian, Jinhong Li, Xinmin, Weimin Guan, Yong Deng, Lei Ning. Enhanced thermal conductivity of PEG/diatomite shape-stabilized phase change materials with Ag nanoparticles for thermal energy storage. Journal of materials chemistry A 3 (2015) 8526-8536.

[8] Ci Ao, Suying Yan, Long Zhao, Xiaoyan Zhao, Yuting Wu. Design of a stearic acid/boron nitride/expanded graphite multifiller synergistic composite phase change material for thermal

energy storage. Energy and Built Environment 2022, doi.org/10.1016/j.enbenv.2022.04.004.

[9] Chuan Li, Qi Li, Xuekun Lu, Ruihuan Ge, Yanping Du, Yaxuan Xiong. Inorganic salt based shape-stabilized composite phase change materials for medium and high temperature thermal energy storage: Ingredients selection, fabrication, microstructural characteristics and development, and applications. Journal of Energy Storage 55 (2022) 105252.

[10] Yu Du, Haowei Huang, Xinpeng Hu, Shuang Liu, Xinxin Sheng, Xiaolong Li, Xiang Lu, Jinping Qu. Melamine foam/polyethylene glycol composite phase change material synergistically modified by polydopamine/MXene with enhanced solar-to-thermal conversion. Renewable Energy 171 (2021) 1-10.

Xiang Li, Yang Wang, Shuang Wu, Leidong Xie. Preparation and investigation of multicomponent alkali nitrate/nitrate salts for low temperature thermal energy storage. Energy 160 (2018) 1021-1029.

[11] Shuai Zhang, Yuanpeng Yao, Yingai Jin, Zhen Shang, Yuying Yan. Heat transfer characteristics of ceramic foam/molten salt composite phase change material (CPCM) for medium-temperature thermal energy storage. International Journal of Heat and Mass Transfer 196 (2022) 123262.

[12] Shuai Zhang, Ziyuan Li, Yuanpeng Yao, Limei Tian, Yuying Yan. Heat transfer characteristics and compatibility of molten salt/ceramic porous composite phase change material. Nano Energy 100 (2022) 107476.

[13] Haoran Wang, Xiaofeng Ran, Yajuan Zhong, Linyuan Lu, Jun Lin, Gang He, Liang Wang, Zhimin Dai. Ternary chloride salt-porous ceramic composite as a high-temperature phase change material. Energy 238 (2022) 121838.

[14] Adio Miliozzi, Manila Chieruzzi, Luigi Torre. Experimental investigation of a cementitious heat storage medium incorporating a solar salt/diatomite composite phase change material. Applied Energy 250 (2019) 1023-1035.

[15] Yuqiao Liu, Zeyi Jiang, Xinru Zhang, Bingji Wu, Yufeng Shen, Liang Wu, Xinxin Zhang. Steel slag-KNO3 phase change composites for thermal storage at medium-high temperature and solid waste recycling. Materials Chemistry and Physics 301 (2023) 127655.

[16] Wei Lu, Guizhi Liu, Zhibo Xiong, Zhigen Wu, Guanhua Zhang. An experimental investigation of composite phase change materials of ternary nitrate and expanded graphite for medium-temperature thermal energy storage. Solar Energy 195 (2020) 573-583.

[17] Xiong Yaxuan, Yao Chenhua, Ren Jing, Wu Yuting, Xu Qian, Nie Binjian, Li Chuan, Ding Yulong. Waste semicoke ash utilized to fabricate shape-stable phase change composites for building heating and cooling. Construction and Building Materials 361 (2022) 129638.

[18] Xiong Yaxuan, Wang Huixiang, Wu Yuting, Zhang Jinhua, Li Haimeng, Xu Qian, Zhang Xingxing, Li Chuan, Ding Yulong. Carbide slag based shape-stable phase change materials for waste recycling and thermal energy storage. Journal of Energy Storage 50 (2022) 104256.

[19] Zhu Jiang, Guanhui Leng, Feng Ye, Zhiwei Ge, Chuanping Liu, Li Wang, Yun Huang, Yulong Ding. Form-stable $LiNO_3$-$NaNO_3$-KNO_3-$Ca(NO_3)_2$/calcium silicate composite phase change material (PCM) for mid-low temperature thermal energy storage. Energy Conversion and Management 106 (2015) 165-172.

[20] Qi Li, Wenzhen Wei, Yuying Li, Chuan Li, Ruihuan Ge, Yanping Du, Xinjing Zhang, Yuting Wu. Development and investigation of form-stable quaternary nitrate salt based composite phase change material with extremely low melting temperature and large temperature range

for low-mid thermal energy storage. Energy Reports 8 (2022) 1528-1537.
[21] Chuan Li, Qi Li, Lin Cong, Feng Jiang, Yanqi Zhao, Chuanping Liu, Yaxuan Xiong, Chun Chang, Yulong Ding. MgO based composite phase change materials for thermal energy storage: The effects of MgO particle density and size on microstructural characteristics as well as thermophysical and mechanical properties. Applied Energy 250 (2019) 81-91.
[22] Chuan Li, Qi Li, Lin Cong, Yongliang Li, Xianglei Liu, Yimin Xuan, Yulong Ding. Carbonate salt based composite phase change materials for medium and high temperature thermal energy storage: A microstructural study. Solar Energy Materials and Solar Cells 196 (2019) 25-35.
[23] Yaojie Tang, Di Su, Xiang Huang, Guruprasad Alva, Lingkun Liu, Guiyin Fang. Synthesis and thermal properties of the MA/HDPE composites with nano-additives as form-stable PCM with improved thermal conductivity. Applied Energy 180 (2016) 116-129.
[24] Sarinthip, Thanakkasaranee, Jongchul Seo. Effect of halloysite nanotubes on shape stabilities of polyethylene glycol-based composite phase change materials. International Journal of Heat and Mass Transfer 132 (2019) 154-161.
[25] Cuneyt Erdinc Tas, Hayriye Unal. Thermally buffering polyethylene/halloysite/phase change material nanocomposite packaging films for cold storage of foods. Journal of Food Engineering 292 (2021) 110351.
[26] Qi Li, Lin Cong, Xusheng Zhang, Bo Dong, Boyang Zou, Zheng Du, Yaxuan Xiong, Chuan Li. Fabrication and thermal properties investigation of aluminium based composite phase change material for medium and high temperature thermal energy storage. Solar Energy Materials and Solar Cells 211 (2020) 110511.
[27] Yan Zhou, Dekun Sheng, Xiangdong Liu, Changhong Lin, Fance Ji, Li Dong, Shaobin Xu, Yuming Yang. Synthesis and properties of crosslinking halloysite nanotubes/polyurethane-based solid-solid phase change materials. Solar Energy Materials and Solar Cells 174 (2018) 84-93.
[28] Hengxue Xiang, Jialiang Zhou, Yangkai Zhang, Mugaanire Tendo Innocent, Meifang Zhu. Polyethylene glycol infused acid-etched halloysite nanotubes for melt-spum polyamide-based composite phase change fibers. Applied Clay Sicence 182 (2019) 105249.
[29] Yi Wang, Ziyi Qin, Ting Zhang, Deyi Zhang. Preparation and thermophysical properties of three-dimensional attapulgite based composite phase change materials. Journal of Energy Storage 32 (2020) 101847.
[30] Xiaobin Gu, Peng Liu, Changjiang Liu, Lihua Peng, Huichao He. A novel form-stable phase change material of palmitic acid-carbonized pepper straw for thermal energy storage. Materials Letters 248 (2019) 12-15.
[31] Ang Li, Jingjing Wang, Cheng Dong, Wenjun Dong, Dimberu G. Atinafu, Xiao Chen, Hongyi Gao, Ge Wang. Core-sheath structural carbon materials for integrated enhancement of thermal conductivity and capacity. Applied Energy 217 (2018) 369-376.
[32] Xiwen Jia, Qingye Li, Chenghong Ao, Rui Hu, Tian Xia, Zhouhang Xue, Qunhao Wang, Xueyong Deng, Wei Zhang, Canhui Lu. High thermal conductive shape-stabilized phase change materials of polyethylene glycol/boron nitride@ chitosan composites for thermal energy storage. Composites Part A: Applied Science and Manufacturing 129 (2020) 105710.
[33] Haiyan Wu, Sha Deng, Yaowen Shao, Jinghui Yang, Xiaodong Qi, Yong Wang. Multiresponsive shape-adaptable phase change materials with cellulose nanofiber/graphene nanoplatelet hybrid-coated melamine foam for light/electro-to-thermal energy storage and

utilization. ACS applied materials & interfaces 11 (2019) 46851-46863.

[34] Xiaosheng Du, Jinghong Qiu, Sha Deng, Zongliang Du, Xu Cheng, Haibo Wang. Alkylated nanofibrillated cellulose/carbon nanotubes aerogels supported form-stable phase change composites with improved n-alkanes loading capacity and thermal conductivity. ACS applied materials & interfaces 12 (2020) 5695-5703.

[35] Dan Li, Xiaomin Cheng, Yuanyuan Li, Haiyuan Zou, Guoming Yu, Ge Li, Yi Huang. Effect of MOF derived hierarchical Co3O4/expanded graphite on thermal performance of stearic acid phase change material. Solar Energy 171 (2018) 142-149.

[36] Zekun Wang, Xiaoguang Zhang, Yunfei Xu, Guo Chen, Fankai Lin, Hao Ding. Preparation and thermal properties of shape-stabilized composite phase change materials based on paraffin wax and carbon foam. Polymer 237 (2021) 124361

[37] Jie Yang, Guo-Qiang Qi, Yang Liu, Rui-ying Bao, Zheng-Ying Liu, Wei Yang, Bang-Hu Xie, Ming-Bo Yang. Hybrid graphene aerogels/phase change material composites: Thermal conductivity, shape-stabilization and light-to-thermal energy storage. Carbon, 100 (2016) 693-702.

[38] C. Yang, M.E. Navarro, B. Zhao, G. Leng, G. Xu, L. Wang, Y. Jin, Y. Ding. Thermal conductivity enhancement of recycled high density polyethylene as a storage media for latent heat thermal energy storage. Solar Energy Materials and Solar Cells 152 (2016) 103-110.

[39] Argyrios Anagnostopoulos, Maria Elena Navarro, Maria Stefanidou, Yulong Ding, Georgios Gaidajis. Red mud-molten salt composites for medium-high temperature thermal energy storage and waste heat recovery applications. Journal of Hazardous Materials 413 (2021) 125407.